HHS Public Access

Author manuscript

IEEE Trans Biomed Eng. Author manuscript; available in PMC 2017 December 12.

Published in final edited form as:

IEEE Trans Biomed Eng. 2017 June ; 64(6): 1211–1217. doi:10.1109/TBME.2016.2595525.

Energy Dissipation in Ex-Vivo Porcine Liver during Electrosurgery

Wafaa Karaki, **Ali Akyildiz**, **Suvranu De**, and **Diana-Andra Borca-Tasciuc**

Department of Mechanical, Aerospace and Nuclear Engineering, Rensselaer Polytechnic Institute, Troy, NY, USA

Abstract

This paper explores energy dissipation in ex-vivo liver tissue during radiofrequency current excitation with application in electrosurgery. Tissue surface temperature for monopolar electrode configuration is measured using infrared thermometry. The experimental results are fitted to a finite element model for transient heat transfer taking into account energy storage and conduction in order to extract information about “apparent” specific heat, which encompasses storage and phase change. The average apparent specific heat determined for low temperatures is in agreement with published data. However, at temperatures approaching the boiling point of water, apparent specific heat increases by a factor of five, indicating that vaporization plays an important role in the energy dissipation through latent heat loss.

Index Terms

electrosurgery; inverse finite element; liver ablation; specific heat

I. Introduction

AN accurate understanding of heat transfer and temperature variation in soft tissue during electrosurgical procedures can help simulate and predict areas of tissue damage and necrosis. Electrosurgery is the application of radiofrequency (300kHz-5MHz) alternating current to achieve tissue effects including cutting, ablation, and desiccation. Studies on safety of electrosurgical procedures and the design of new and improved electrosurgical tools often utilize finite element modeling and tissue properties reported in literature to predict temperature variations [1][2]. However, computational results deviate significantly from experimental data. One of the main challenges for accurate simulation and temperature prediction lies with the accurate modeling of energy dissipation and storage processes that can be affected by temperature, frequency, and water content [3][4][5]. Another important challenge is the lack of accurate knowledge of tissue thermal properties including specific heat and thermal conductivity for a wide temperature range encountered in electrosurgery. While inaccuracy of thermal conductivity may be of lesser importance, as tissue heating is rapid and heat conduction is not the dominant mode of energy dissipation, the lack of high temperature specific heat values is critical. Soft tissue thermal property characterization

Correspondence to: Diana-Andra Borca-Tasciuc.

often assumes temperature independent properties and is limited to measurements at room or body temperatures [6][7][8][9].

Only a few studies have considered the effect of temperature dependence of specific heat. Haemmerich et al. characterized specific heat of ex-vivo liver up to 85 °C. Specific heat was found to remain unchanged until 70 °C, after which it increased. This increase was attributed to the effects of coagulation and water loss [10]. Choi et al. measured the temperature dependent thermal properties for fresh and preheated porcine liver by heating it up to 85 °C. Their measurements of apparent specific heat showed a slight increase due to protein denaturation and a decrease with lower water content. Their study focused strictly on specific heat and excluded latent heat loss due to water content loss by conducting tests in an enclosed aluminum pan where the water content of the liver did not change during heating [11].

However, evaporation and the associated latent heat loss can have a significant effect on the temperature rise in tissue undergoing RF heating, which is the main challenge to develop accurate models for electrosurgery. Surprisingly, this energy dissipation mechanism, which should play a dominant role in electrosurgery, where temperatures exceed 100 °C [12][13], is often neglected in literature and only a few studies recognize its importance in electrosurgery or similar energy based surgical methods [3][12][15]. For instance, Yang et al. measured the water content of liver tissue after an ablation process by cutting liver into 5mm × 5mm × 1 mm sections and weighing them before and after vacuum drying. They correlated the water content variation with temperature, and fitted it with an approximate numerical model [14]. In another study by the same group, Pennes bioheat equation was modified to include water evaporation as a function of temperature during ablation within an apparent specific heat term. The model was shown to better predict the experimental temperature data when boiling temperature of water was approached [15]. Chen et al. used Yang's effective specific heat in modeling vessel sealing in bipolar electrosurgery at high temperatures [3]. The authors note that an assumed numerical model for water loss affecting the apparent specific heat had to be made at temperatures exceeding 103 °C as no experimental data was found in literature.

While other energy dissipation mechanisms including coagulation and thermal decomposition are also expected to play a role, water makes up more than 70% of soft tissue content by mass [6] and has a very high latent heat of vaporization [3]. Thus, its evaporation from the tissue should play a dominant role in energy dissipation at elevated temperatures. In this paper, we determine the variation in apparent specific as a function of temperature during monopolar radiofrequency heating of ex-vivo liver tissue. In addition to heat storage inside tissue, apparent specific heat assessed here also captures the effects of energy dissipation via coagulation and phase change. For this purpose, experimental measurements of surface temperature are collected at multiple power settings. A finite element model is used to fit the data in an iterative approach to find the temperature-dependent apparent specific heat. Results are compared with data found in literature for specific heat at or around room temperature. A few other aspects are also illustrated and discussed, such the power dependence of apparent specific heat.

II. Method

A. Experimental Procedure

Experiments were carried out on single lobes from four different samples of fresh porcine liver purchased locally less than 48 hours post-slaughter. Samples were kept in thermal insulation during transportation from the vendor and then preserved via static cold storage at 4 °C prior to start of the experiment. During experiments, each liver was placed on a dispersive return pad (ESU Ground Pad 400-2100, Conmed Corporation, Utica, NY) and good electrical contact was ensured. An infrared (IR) camera (FLIR A655sc) with a 480p × 640p resolution and 30 Hz data acquisition rate was positioned above the tissue and set to record temperature (Fig. 1). The infrared radiation wavelength λ_1 emitted due to the temperature of the liver is estimated to be 8-10 μm from Wien's Law, and the penetration depth $(\alpha(\lambda_1)^{-1}$, where α is the absorption coefficient) is calculated to be 6-12 μm [16][17]. Thus, the temperature captured by the IR camera is considered to be the surface temperature. A single image of a 10 mm × 10 mm square was first taken to measure the pixel to mm scale for each measurement. A 1.17 mm radius bent ball-tip electrode (Electrosurgical Ball Electrode A831, Bovie Medical Corporation, Clearwater, FL) was used to perform stationary ablation on the liver using an electrosurgical unit (System 2450 ® Electrosurgical Generator, Conmed Corporation). To prevent drying of the liver surface, application of saline solution was attempted first. This is often used in electrosurgery [18] with the same purpose, however here it was found to create unintended current pathways and resulted in hot spots far from the electrode. Thus to prevent drying of the liver surface, the samples were instead covered with a thin plastic film until the ablation process. A region of least 30 mm in radius surrounding the electrode was exposed to the ambient during each measurement.

The electrode was held by a robotic arm (Universal Robots, Setauket, NY) at an angle to allow an unobstructed top view for the IR camera as shown in Fig. 1. A 400 kHz sinusoidal "pure cut" signal was applied at different power settings. The voltage waveform generated by the electrsosurgical unit (ESU) was measured using an oscilloscope (Agilent MSOX2024A) along with the RMS equivalent. The current was found by measuring the voltage drop across a 10 Ω resistor placed in series with the tissue. The power generated by the ESU was calculated from the RMS of the voltage and current ($P = V_{rms}I_{rms}$) measured at each power setting and was found to be within 5% of the nominal power rating for all measurements. At each measurement, the electrode was placed in contact with the tissue and activated for 5 seconds. Infrared video of the temperature field was acquired for a total of 30 seconds for each measurement. This process was repeated for power settings of 10, 25, 30, and 50 Watts for each liver specimen, at different spatial locations on the liver.

The location of the electrode was identified from the infrared images. At each infrared image frame corresponding to time instant t, temperatures at points with the same radial distance from the tip of the electrode were averaged to compute the radial temperature profile.

B. Governing Equations

The temperature and electric field distributions inside the tissue are governed by the coupled conservation of energy and conservation of charge laws. Conservation of energy for this problem yields the following equation:

$$-\nabla \cdot \mathbf{q}(\mathbf{x},\mathrm{t})+\dot{q}_e(\mathbf{x},\mathrm{t})=\frac{\partial H}{\partial t}(\mathbf{x},\mathrm{t}) \quad (1)$$

where **q**(**x**, t) in (W/m^2), *H*(**x**, t) in (J/kg), $\dot{q}_e(\mathbf{x},\mathrm{t})$ (W/m^3) denote the thermal flux, enthalpy, and heat generation due to Joule heating respectively at a point **x** and time *t* (s) in the system. Expressing the internal energy change in terms of the "apparent" volumetric heat capacity ρc_{app} and using Fourier's law,

$$\mathbf{q}(\mathbf{x},\mathrm{t})=-k\nabla T(\mathbf{x},\mathrm{t}) \quad (2)$$

Equation (1) may then be written as,

$$\nabla \cdot k\nabla T(\mathbf{x},\mathrm{t})+\dot{q}_e(\mathbf{x},\mathrm{t})=\rho \mathrm{c}_{\mathrm{app}}\frac{\partial T}{\partial t}(\mathbf{x},\mathrm{t}) \quad (3)$$

where *k* is the temperature dependent thermal conductivity (W/m·K), *T* is the temperature (K), ρ is the density (kg/m^3) and *capp* is the apparent specific heat of the tissue (J/kg·K). The apparent specific heat (c_{app}) is not the true specific heat but includes the effects of energy losses due to vaporization and coagulation.

Conservation of electrical charge provides the equation for the potential distribution in the tissue,

$$\nabla \cdot \sigma \nabla V=0 \quad (4)$$

where σ is the temperature dependent electrical conductivity (S/m), and *V* is the electric potential (V). The heat generated due to radiofrequency electrical excitation $\dot{q}_e(\mathrm{W/m^3})$ is:

$$\dot{q}_e=\boldsymbol{J}\cdot\boldsymbol{E} \quad (5)$$

where ***J*** is the current density (A/m^2) and ***E*** is the electric field (V/m):

$$\boldsymbol{E}=\nabla V \quad (6)$$

At the frequency used in electrosurgical procedures, capacitive losses are negligible and heat generation can be considered to be mainly resistive [3]. The electric field and current density are related by:

$$\boldsymbol{J}=\sigma \boldsymbol{E}. \quad (7)$$

C. Finite Element Model

The commercial software package Abaqus v6.13 (Dassault Systèmes Americas Corp, Waltham, MA) was used to solve the above equations numerically on an axis-symmetric 30 mm × 30 mm finite element model of the tissue as shown in Figure 2. The electrode was modeled with a contact tip radius of re = 1.17 mm and 10 mm length to match the ball-tip electrode used in the experiments. An equivalent root-mean-square (RMS) current source was applied across the top of the electrode and a zero potential was defined at the bottom boundary of the liver. A convection boundary condition was defined at the top surface (h = 3.1 W/m^2·K[19]) and a zero heat flux (insulation) at the outer and bottom boundaries as shown in Fig. 2. A non-uniform mesh consisting of 8-noded quadratic axisymmetric elements was used with smaller elements close to the electrode-tissue interface where large temperature gradients are expected. Convergence of the solution was verified by increasing the number of elements.

Temperature dependent electrical conductivity $\sigma(T)$ [20] and thermal conductivity $k(T)$ [21] of tissue and electrodes were obtained from literature and are shown in Table I. During simulations, linear interpolation is used to compute $\sigma(T)$ and $k(T)$ at temperature T. Since no experimental data is available for either property above 100 °C, it is assumed that both properties of tissue remain constant beyond this temperature. The electrical contact resistance between the electrode and tissue interface was approximated by finding the difference between the total resistance determined from voltage and current experimental measurements ($R_{total} = V_{rms}/I_{rms}$) and estimated tissue resistance assuming a hemispherical contact in a semi-infinite medium ($R_{tissue} = 1/(\pi r_e \sigma)$). The electrical contact resistance was found to vary between 10 and 50 Ω which is comparable with prior measurements of electrode-cardiac tissue contact resistance [22]. Thermal contact resistance was assumed to be of the order of 0.001 m^2.K/W [3].

The apparent specific heat (c_{app}) of the tissue, which is discussed next, was determined iteratively by minimizing the difference between the temperature distribution measured in the experiments and simulation data at five different time points for the same radial location on the tissue measured from the tip of the electrode. The trust-region-reflective algorithm as implemented in Matlab R2014a (MathWorks, Natick, MA) was utilized to minimize the difference between the experimentally measured and computed temperatures expressed by the following objective function, f:

$$f=\sum_{i=1}^{n}\left(T_i^{\text{measured}}-T_i^{\text{computed}}\right)^2 \quad (8)$$

where T_i represents the temperature at radial location (r_i) of a measurement point at time 't_i' and n is the total number of such measurement points which is between 125 and 135. The termination criterion for the iterations was set as $\Delta f \leq 10^{-6}$.

Based on temperature-dependent specific heat data available in literature [10] c_{app} is expected to behave linearly with temperature and change its slope at 80°C, where protein coagulation and vaporization begin to have an effect, and again at 100°C which corresponds to the boiling temperature of water. Therefore, the apparent specific heat was modeled as a continuous piece-wise linear function of temperature as shown in (9):

$$c_{\mathrm{app}}(T)=\begin{cases} c_1 & T<37^{\circ}\mathrm{C} \\ \left(\frac{c_2-c_1}{43}\right)T+c_1 & 37^{\circ}\mathrm{C}\leq T<80^{\circ}\mathrm{C} \\ \left(\frac{c_3-c_2}{20}\right)T+c_2 & 80^{\circ}\mathrm{C}\leq T<100^{\circ}\mathrm{C} \\ \left(\frac{c_4-c_3}{20}\right)T+c_3 & 100^{\circ}\mathrm{C}\leq T<120^{\circ}\mathrm{C} \end{cases} \quad (9)$$

where c_1, c_2, c_3, and c_4 are the values of $c_{app}(T)$ at 37, 80, 100, and 120°C respectively. The fitting was carried out sequentially in order to optimize computational time and convergence, first considering temperature data in the range < 80°C and then in the range 80 °C –120 °C. During fitting, the experimental axis-symmetric radial temperature profiles in the range < 80°C at five time steps were obtained from each measurement location (by circumferentially averaging the temperature at each radius considered) and fitted to the temperature predicted by the finite element model. The apparent specific heat $c_{app}(T)$ was evaluated for each data point and the parameters c_1 and c_2 were found by minimizing the objective function in Eq. 8. Next, images with temperature data in the range (80 °C –120 °C) were analyzed, in a similar manner. During this second fitting process c_3 and c_4 were found. The search range and initial guesses for the parameters are listed in Table II.

D. Sensitivity Analysis

The sensitivity of the solution to quantities including the electrical conductivity (σ), thermal conductivity (k), and the apparent specific heat (c_{app}) has been analyzed by defining the following error measure:

$$\varepsilon(T)=\sqrt{\frac{\sum_{i=1}^{\mathrm{n}}\left(T_{\mathrm{ref},i}-T_i\right)^2}{\sum_{i=1}^{\mathrm{n}}\left(T_{\mathrm{ref},i}\right)^2}} \quad (10)$$

where T_{ref} is the reference temperature profile obtained from the solution of equation (3) when using liver properties from literature [6], σ = 0.33 S/m, k = 0.518 W/m·K and c_{app} = 3600 J/kg·K along with experimental parameters, i.e. electrode radius of 1.17 mm and 25W applied power. A similar error measure was used to determine the sensitivity of the solution to the contact area between the electrode and the tissue, which is a function of the radius (r_e) of the tip of the ball electrode. In that analysis, electrodes of various radii ranging from 0.15 mm to 3.0 mm were input into the simulation, while T_{ref} was taken as the profile obtained corresponding to the minimum radius of 0.15 mm.

III. Results and discussion

A. Sensitivity Analysis

The results of the sensitivity analysis are first discussed in this section. Fig. 3(a) shows the error $\varepsilon(T)$ as function of the radius of the electrodes. The results show that the error plateaus as the electrode radius is increased. This guided the selection of the electrode diameter from commercially available options to a 3/32 inch (2.38mm) ball electrode with measured diameter of 2.34 ± 0.05 mm. At this diameter, an uncertainty in the diameter measurement of ±0.05 mm produces an uncertainty in the predicted temperature distribution of less than ±0.7%.

The sensitivity of the temperature distribution to thermal conductivity, electrical conductivity and specific heat are shown in Fig. 3(b). The results are found to have low sensitivity to changes in thermal conductivity. Reported measurements of k in literature [6] were found to vary at most by 30% from the mean values used in this study. A 30% change in k while keeping all other parameters constant results in less than 1°C average change in temperature profile. This may be due to the fast heating process in which temperature rise occurs in a time interval of less than 2 seconds. Thus, conduction does not appear to be the dominant mode of energy dissipation and thermal conductivity is not a critical parameter in the simulation of radiofrequency electrical heating of tissue. Therefore, the errors associated with assuming the thermal conductivity data from literature are expected to be small.

While there is a weak dependence of the solution on changes in thermal conductivity, the temperature varies more strongly with electrical conductivity and heat capacity Similar to thermal conductivity measurements, reported measurements of σ in the literature did not vary by more than 30% including outliers. As seen in Fig. 3b, a change in σ by 30% results in a ~30% change in the specific heat and in > 7°C average change in temperature, which can have a significant effect on the outcome of an electrosurgical procedure. These results highlight the importance of using accurate temperature dependent parametrization of σ and c to model heat dissipation in electrosurgery. As with any biological tissue, variability in physical properties due to physiology is expected between different tissue samples which may depend on multiple factors including the animal size, age, gender, breed and diet. To address this uncertainty, measurements were done on multiple liver samples and repeated at multiple power settings with the means and standard deviations of the results reported.

B. Experimental Results

Representative data of the experimentally observed temperature distribution is shown in Fig. 4(a) for a single measurement at 25W power setting before the electrode is activated and at five different time steps for a total time of 0.594 s following activation. The images shown in this figure correspond to temperature data in the 30-80 C temperature interval. The first frame shows the region of interest (ROI) and the location of the electrode. The other frames illustrate the evolution of the temperature profile with time. The temperature distribution shows axial symmetry which is also observed at lower power settings (10W, 25W, and 30W). Fig. 4(b) shows the averaged temperature profile as a function of radial distance from the center of the electrode for all five time steps in Fig 4(a). The corresponding

computationally obtained temperature profiles after minimizing the error for the parameters c_1 and c_2 in temperature dependent c_{app} are shown in dashed lines. The averaged temperature profile as a function of radial distance from the center of the electrode at five time steps was also obtained for the 80-120 °C temperature range and similarly used to find c_3 and c_4. A representative of the high temperature data is shown in Fig. 5 as solid lines for IR recording at 25W power setting at a single location; the dashed lines are the predicted temperature profiles after minimizing the error.

The mean apparent specific heat and the standard deviation for the 10, 25, 30 and 50W power settings at the four temperature points are shown in Table III. Fig. 6 shows c_{app} plotted against temperature for the four power settings and compared against literature. At 37°C, there is little variability found between measurements (c_{app} = 3659 J/kg·K) within and across the power settings. This value compares well with values reported for porcine liver which range from 3060 J/kg·K to 3870 J/kg·K [6][10]. However, as the temperature increases, the apparent specific heat increases significantly. The values of c_{app} observed at 80°C were found to be higher than that measured by Choi et al. [11] which was expected since the latter does not include water content losses due to vaporization. The increase in c_{app} peaks at a temperature of 100°C, the boiling point of water. This effect is attributed to an increasing rate of water evaporative losses and phase change that peaks at the boiling point. A decrease in the specific heat at 120°C is then observed which can be explained by the decrease in the amount of the water in the liver free to evaporate. The temperature did not significantly exceed 100°C in the 10W and 50W case so the c_4 parameter for those cases could not be computed. In the 10W case, the power density is too low to go over the boiling temperature, whereas in the 50W case, due to the high power density, charring at the electrode tissue interface occurred after approximately 0.5 s which interrupted the heating process and further data could not be collected.

The peak in the specific heat due to vaporization losses matches the model proposed by Chen et al. [3] but is significantly smaller in magnitude. The model by Chen et al. is based on water content measurements done by Yang et al. [14] on porcine liver tissue. Yang et al. determined the water loss by cutting the tissue and weighing it before and after vacuum drying, and noted that samples with remaining water content greater than 50% could not be measured due to a noticeable water drip in their method. It is unclear whether this effect could have been present to some degree in measurements on samples with less than 50% water content. In addition, in their experiment, the tissue was heated for a total of 6 minutes, in contrast with 2 s of heating in the present work. This could be another explanation for the observed differences, since a longer process will allow more water to evaporate. This large difference highlights the need for accurate models that describe the energy losses due to phase change and water loss in biological tissue during electrosurgery.

IV. Conclusion

This study investigates energy dissipation process in electrosurgery and presents a method to determine apparent specific heat over a wide temperature range during radiofrequency heating of tissues. Results show a large increase in c_{app} and a peak at 100°C attributed mainly to water vaporization and latent heat loss. These results, coupled with sensitivity

analysis, indicate that energy dissipation, especially at temperatures approaching boiling, is dominated by energy storage and latent heat loss. The peak in the apparent specific heat due to vaporization losses at the boiling point was found to be significantly smaller than that in proposed literature models. Results indicate that more accurate models are needed which take into account phase change.

Acknowledgments

We gratefully acknowledge the helpful suggestions and comments of Dr. Carlos Lopez.

This work was supported by the U.S. National Institute of Health NIH/NIBIB 1R01EB014305.

References

1. Chang IAJ. Considerations for thermal injury analysis for RF ablation devices. The open biomedical engineering journal. 2010 Feb.4:3. [PubMed: 20300227]
2. Dodde RE, Gee JS, Geiger JD, Shih AJ. Monopolar electrosurgical thermal management for minimizing tissue damage. Biomedical Engineering, IEEE Transactions on. 2012 Jan; 59(1):167–173.
3. Chen RK, Chastagner MW, Dodde RE, Shih AJ. Electrosurgical Vessel Sealing Tissue Temperature: Experimental Measurement and Finite Element Modeling. Biomedical Engineering, IEEE Transactions on. 2013 Feb; 60(2):453–460.
4. Berjano EJ. Theoretical modeling for radiofrequency ablation: state-of-the-art and challenges for the future. Biomedical engineering online. 2006 Apr.5(1):24. [PubMed: 16620380]
5. Chang I. Finite element analysis of hepatic radiofrequency ablation probes using temperature-dependent electrical conductivity. Biomedical engineering online. 2003 May.2(1):12. [PubMed: 12780939]
6. Duck, FA. Physical properties of tissues: a comprehensive reference book. Academic press; 2013.
7. Cooper TE, Trezek GJ. Correlation of thermal properties of some human tissue with water content. Aerospace medicine. 1971 Jan; 42(1):24–27. [PubMed: 5541087]
8. Valvano JW, Allen JT, Bowman HF. The simultaneous measurement of thermal conductivity, thermal diffusivity, and perfusion in small volumes of tissue. Journal of biomechanical engineering. 1984 Aug; 106(3):192–197. [PubMed: 6492763]
9. Giering K, Lamprecht I, Minet O, Handke A. Determination of the specific heat capacity of healthy and tumorous human tissue. Thermochimica acta. 1995 Mar.251:199–205.
10. Haemmerich D, Santos ID, Schutt DJ, Webster JG, Mahvi DM. In vitro measurements of temperature-dependent specific heat of liver tissue. Medical engineering and physics. 2006 Mar; 28(2):194–197. [PubMed: 16002318]
11. Choi J, Morrissey M, Bischof JC. Thermal processing of biological tissue at high temperatures: impact of protein denaturation and water loss on the thermal properties of human and porcine liver in the range 25–80 C. Journal of Heat Transfer. 2013 May.135(6):061302.
12. Sankaranarayanan G, Resapu RR, Jones DB, Schwaitzberg S, De S. Common uses and cited complications of energy in surgery. Surgical endoscopy. 2013 Sep; 27(9):3056–3072. [PubMed: 23609857]
13. Massarweh NN, Cosgriff N, Slakey DP. Electrosurgery: history, principles, and current and future uses. Journal of the American College of Surgeons. 2006 Mar; 202(3):520–530. [PubMed: 16500257]
14. Yang D, Converse MC, Mahvi DM, Webster JG. Measurement and analysis of tissue temperature during microwave liver ablation. Biomedical Engineering, IEEE Transactions on. 2007 Jan; 54(1): 150–155.
15. Yang D, Converse MC, Mahvi DM, Webster JG. Expanding the bioheat equation to include tissue internal water evaporation during heating. Biomedical Engineering, IEEE Transactions on. 2007 Aug; 54(8):1382–1388.

16. Nordal PE, Kanstad SO. Photothermal radiometry. Physica Scripta. 1979; 20(5-6):659.
17. Bertie JE, Lan Z. Infrared Intensities of Liquids XX: The Intensity of the OH Stretching Band of Liquid Water Revisited, and the Best Current Values of the Optical Constants of H 2 O (l) at 25° C between 15,000 and 1 cm-1. Applied Spectroscopy. 1996; 50(8):1047–1057.
18. Donzelli J, Leonetti JP, Bergstrom R, Wurster R, Young MRI. Thermoprotective mechanisms of irrigation during bipolar cautery. Otolaryngology–Head and Neck Surgery. 1997 Aug; 117(2):103–104.
19. de Dear RJ, Arens E, Hui Z, Oguro M. Convective and radiative heat transfer coefficients for individual human body segments. International Journal of Biometeorology. 1997 May; 40(3):141–156. [PubMed: 9195861]
20. Zurbuchen U, Holmer C, Lehmann KS, Stein T, Roggan A, Seifarth C, Buhr HJ, Ritz JP. Determination of the temperature-dependent electric conductivity of liver tissue ex vivo and in vivo: Importance for therapy planning for the radiofrequency ablation of liver tumours. International Journal of Hyperthermia. 2010 Jan; 26(1):26–33. [PubMed: 20100050]
21. Bhattacharya A, Mahajan RL. Temperature dependence of thermal conductivity of biological tissues. Physiological measurement. 2003 Jul.24(3):769. [PubMed: 14509313]
22. Benzing G, Iltis R, Helmsworth JA, Schreiber T, Kaplan S. Measurement of the ohmic electrode-tissue contact resistance and the voltage applied to myocardium. Journal of biomedical engineering. 1980 Jan; 2(1):3–8. [PubMed: 7359896]

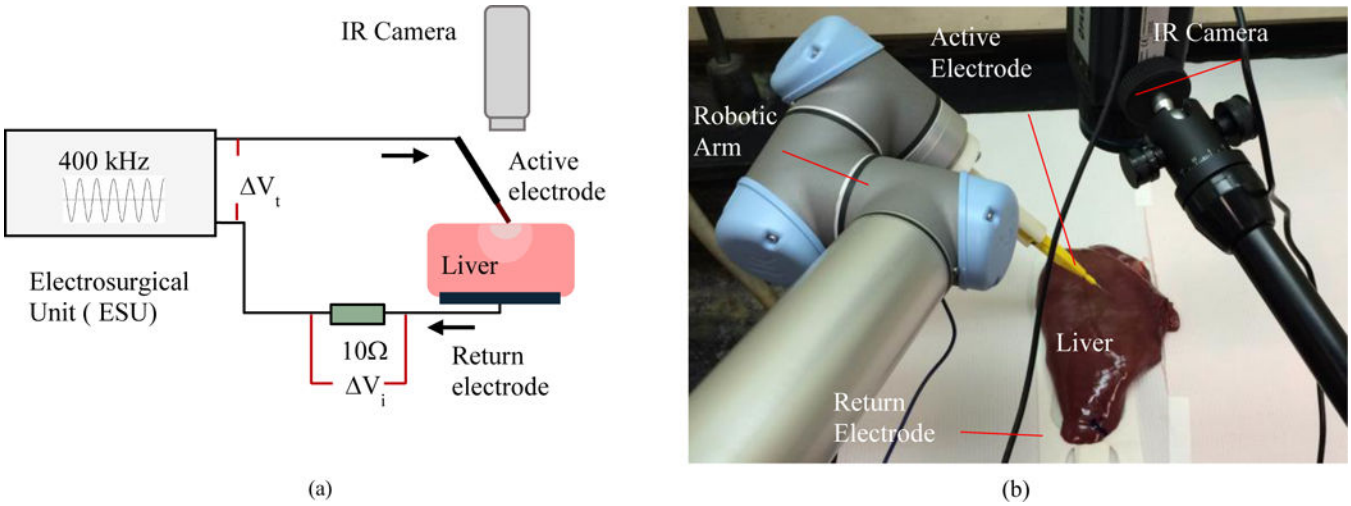

Fig. 1.

(a) Schematic of experimental setup (b) photograph of experiment.

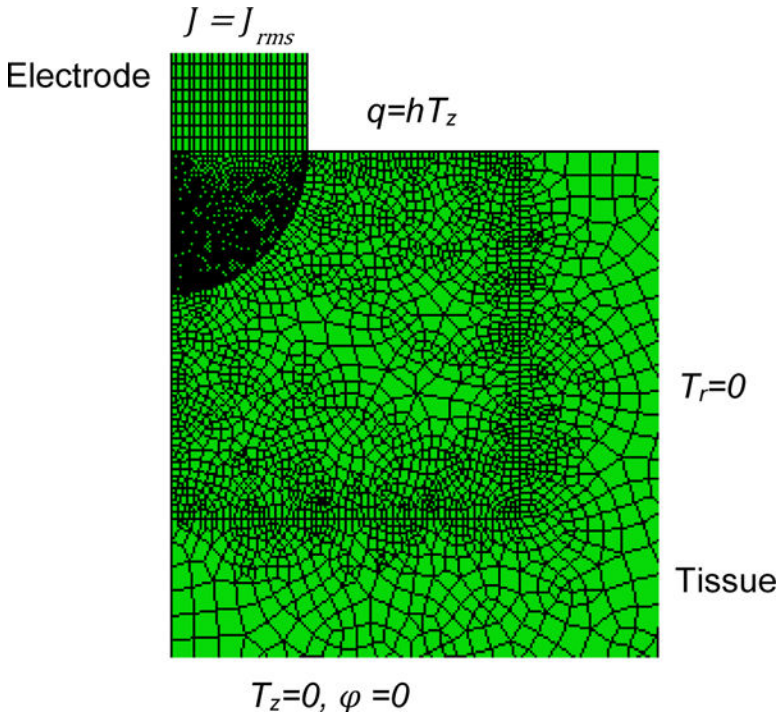

Fig. 2.
Finite element model showing the electrode and tissue with boundary conditions applied.

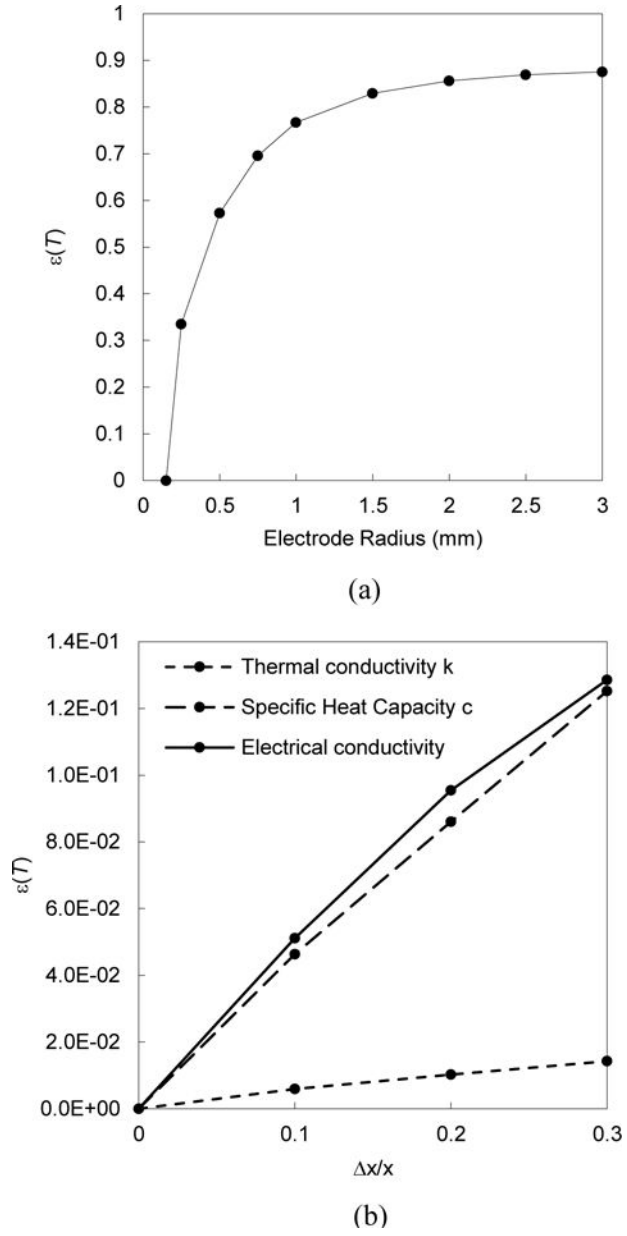

Fig. 3.

Relative error $\varepsilon(T)$ in the computed temperature as a function of (a) electrode radius and (b) $\Delta x/x$, where x stands for k, c or σ.

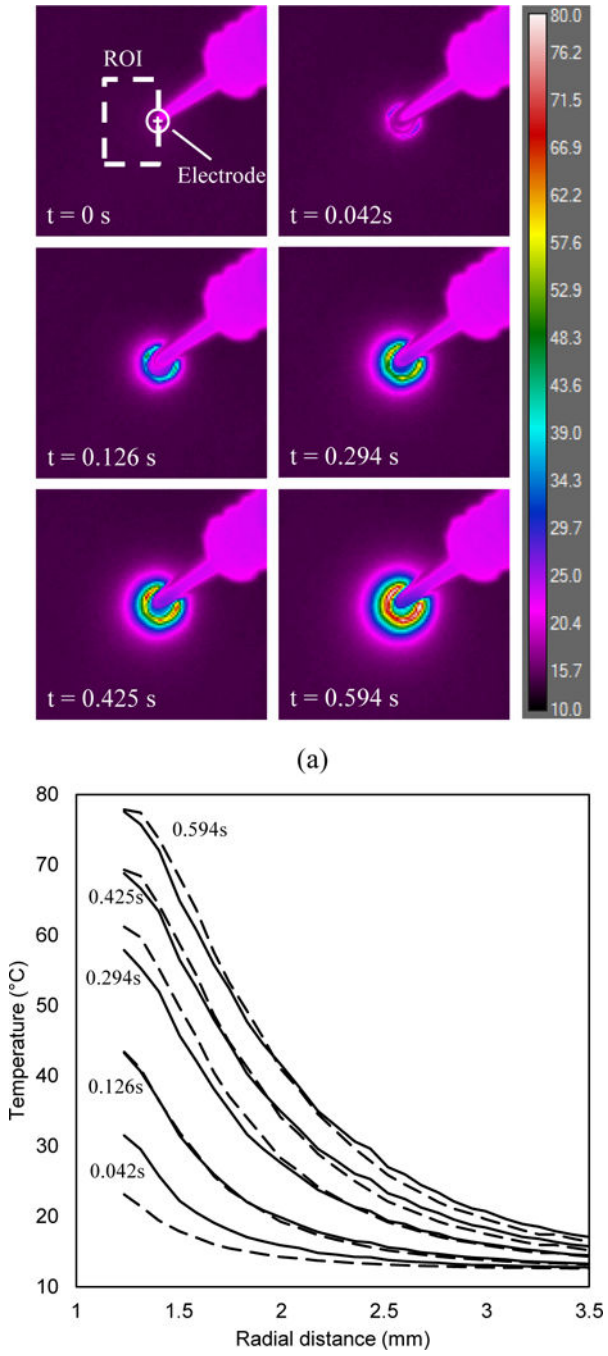

Fig. 4.

(a) Infrared image frames at different time steps corresponding to a single 25W measurement (b) Comparison of mean axis-symmetric radial temperature profile at each time step with simulation after minimization. Radial distance is measured from the center of the electrode.

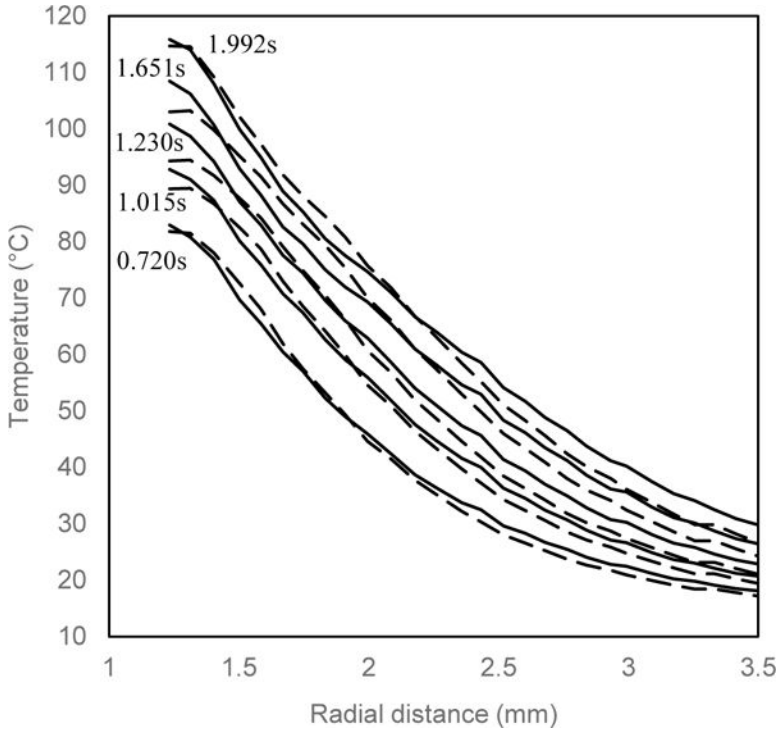

Fig. 5.

Comparison of higher temperature range mean axis-symmetric radial temperature profile for a single 25W measurement at each time step with simulation after minimization. Radial distance is measured from the center of the electrode.

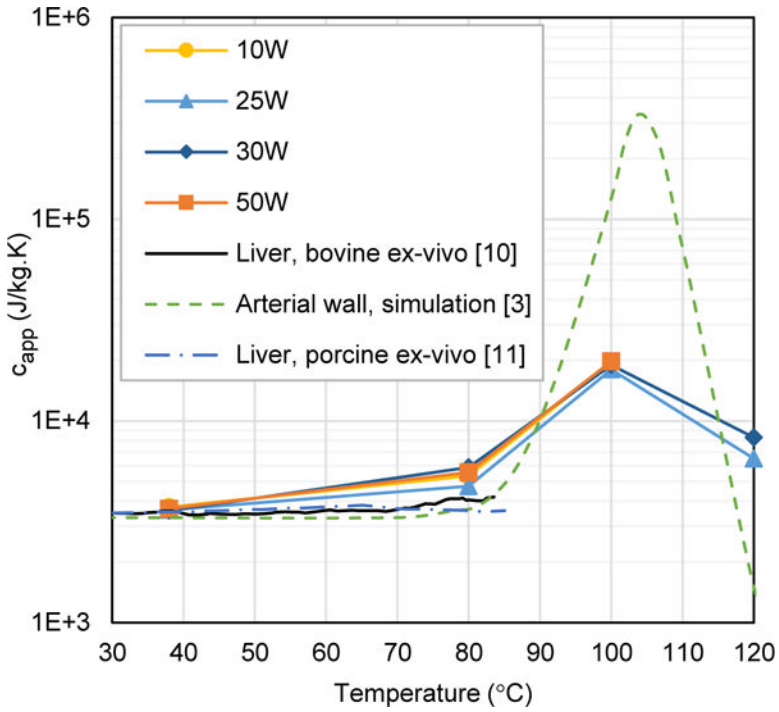

Fig. 6.
Temperature dependent c_{app} compared with the literature.

TABLE I

Physical Properties used in the model

Tissue			
T **(°C)**	**σ(*T*) (S/m)***	***k*(*T*) (W/m.K)****	**ρ (kg/m^3)****
25	0.33	0.518	1070
80	0.79	0.725	
90	0.75	0.73	
100	0.64		
Electrode (Stainless steel)			
$\sigma(T)$ (S/m)	$k(T)$ (W/m.K)	ρ (kg/m^3)	c (kJ/kg·K)
1.4×10^6	11.9	7930	132

*Zurbuchen et al. [20]

**Bhattacharya and Mahajan [21]

TABLE II

Search range and initial guesses for apparent specific heat

Parameter	*T* (°C)	Initial guess (J/Kg.K)	Search range
c_1	37	3.5×10^3	$[1.0\times10^3\ 1.5\times10^4]$
c_2	80	4.5×10^3	$[1.0\times10^3\ 2.5\times10^4]$
c_3	100	1.0×10^4	$[1.0\times10^3\ 1.0\times10^5]$
c_4	120	4.5×10^3	$[1.0\times10^3\ 2.5\times10^4]$

TABLE III

Apparent specific heat for 10, 20, 30 and 50W settings.

Power Setting (W)	**Apparent Specific Heat Capacity c_{app} (J/kg·K)**			
	T = 37°C	T = 80°C	T = 100°C	T = 120°C
	c_1	c_2	c_3	c_4
10 (n = 5)	3740 ± 226	5339 ± 580	19638 ± 2239	N/A
25 (n = 7)	3615 ± 176	4738 ± 582	17977 ± 1405	6516 ± 1036
30 (n = 4)	3589 ± 307	5875 ± 560	18928 ± 1355	8286 ± 413
50 (n = 8)	3629 ± 333	5567 ± 740	19744 ± 1061	N/A
Mean	3659 ± 261	5330 ± 631	19071 ± 1456	7160 ± 810

n is the number of measurements at each power setting.